Bedload transport and its implication on bed morphology at a river confluence

Nabina Khanam
National Institute of Technology Agartala
Sushant Kumar Biswal (sushantb69@gmail.com)
National Institute of Technology Agartala https://orcid.org/0000-0002-1413-7206
Animesh Das
National Institute of Technology Agartala

Research Article

Keywords: Bed morphology, Bedload transport, Field experiments, River confluence

Posted Date: April 4th, 2023

DOI: https://doi.org/10.21203/rs.3.rs-2742429/v1

Abstract

River confluences are the key elements within fluvial systems, where three-dimensional flow fields and sedimentation patterns can have a substantial effect on the hydraulics, bed morphology of stream courses, and environments. The present study is configured to realize the alterations in bedload transportation and in bedform at confluence channel in relation to particular hydrological occurrences. It is anticipated that the patterns of the flow attributes following the confluence to be different from those in the conditions reported in other publication. Therefore, this article concisely reports the various flow aspects, examines the corresponding river bed patterns, and provides a brief description of the different flow properties. On the basis of field findings in response to fluctuation in the flow of contributory tributaries, the recorded morphological and sedimentological changes are explained. To accomplish this, bedload transport, bed surveys, and particle size distribution measurements were carried out at the study site during different hydrological seasons at intervals of two months from January 2018 to March 2019. The three major goals of this work were to comprehend the symmetry between two confluence channels, estimate bedload transport, and investigate the consequences of net fluvial behavior on bedform dynamics. The short-term impacts of stream flow irregularity on channel morphology and particle structures were discovered by repeated transect studies and bed material sampling at a small asymmetrical river junction. Results show that the confluence involves the shifting in the scour region, frequent erosion and deposition of sediments, and bar development at the downstream confluence as flow rate fluctuates following the hydrological changeability in the confluence channels. The average bedload at the confluence appears to be irregular in favor of the tributary, since two-thirds of the total bedload was carried across the shallow zone of the cross-section. A high speed digital camera was used to detect sand ripples, and video technique was utilized to obtain statistics on the presence of ripple geometries. Asymmetric two-dimensional ripples were observed in relatively calm weather conditions and in moderate winds. It was discovered that ripples generated by the two-dimensional flow were supplanted by flatbed circumstances and the normal two-dimensional wash-out ripples after the medium wind periods, demonstrating that the presence of a combined flow increases the induced bed shear stress.

Introduction

A confluence is a location in a fluvial system with complicated hydraulic interaction imparted by the union of two different streams. They form unique dynamic flow environments in which velocity, flow, sediment load and channel bedform change continuously (Biron et al. 1993). The area close to the confluence where this adjustment occurs is called as confluence hydrodynamic zone (CHZ) (Rhoads and Kenworthy 1995). Earlier studies primarily focused on the complex flow structure, secondary circulation, turbulent flow, and distinct geomorphic features within CHZ (Boyer et al., 2006; Rhoads and Sukhodolov, 2001, 2004; Riley and Rhoads 2012; Roy and Bergeron, 1990). Several flow features such as flow deflection, flow stagnation at upstream junction corner, flow separation from the inner bank as branch channel enters the main channel, the mixing interface (MI) among converging streams, spiral motions produced owing to the curvature effect of the branch channel, etc. typically constituted at confluences (e.g., Best, 1987; Biron and Lane, 2008; Bradbrook et al., 2000; Rhoads and Kenworthy, 1998; Rhoads et al., 2009). These features at confluence area depend on various parameters include geometric parameters (channel shape, channel magnitude, confluence angle) and hydraulic parameters (Froude number of flow, momentum ratio in main and branch channel). According to reaserch by (Best, 1987, 1988; Best and Rhoads, 2008; Rhoads and Kenworthy, 1995, 1998), bed morphology at confluences regularly reflects these hydrodynamic zones and exhibits the following characteristics: (1) a scour hole usually aligned along the area of greatest velocity where two streams approach and start to unite; (2) avalanche faces at each tributary mouth that enter the middle scour hole; (3) sedimentation in the stagnation region; and (4) bars developed in the separation region at the lower confluence corner or midstream in the post-confluence channel. Several researchers are interested in studying the flow structure, scouring, and sedimentation at river confluence. According to previous studies, the confluence angle, sediment discharge, and discharge or momentum flux ratios between confluence channels, as well as bed concordance, are the key factors influencing the flow pattern and channel bedform (Best, 1987, 1988; Best and Roy, 1991; Biron et al., 1996, 2002; De Serres et al., 1999; Rhoads and Kenworthy, 1998). Ghobadian and Shafai Bejestan (2007) illustrated that the discharge ratio is the most crucical element to take into account while studying river confluence. Zhang and Lin (2021) examnied the impact of fluctuating the discharge ratio on flow and sediment patterns in a 90° junction channel under the clear water situation. Xia Shen et al. (2022) examined the impact of confluence angles and discharge ratios on the formation and growth of secondary flows, and separation region using numerical model. The findings indicated that twin surface-convergent secondary flows formed on the either sides of the shear plane, while a separation region with low flow velocity generated immediately confluence downstream. When the confluence angle and the discharge ratio vary, the process of secondary flow formation in the separation zone is reversed and becomes very complicated.

Bed morphology is common at river junctions and appears to be a significant factor in the fluvial network that accommodates the difference in bed height between two confluence rivers (bed discordance). Bed discordance is a essential stream morphological characteristic that substantially impact stream discharge, transport of bed material and bedforms (Biron et al., 1996, 2004; Boyer et al. 2006; Sukhodolov et al., 2017). Canelas et al. (2020) characterise the flow behaviour caused by bed discordance at a 70° confluence channel based on detailed quantification of the free surface topography and acoustic Doppler velocimetry (ADV) assessments of 2D velocities under the shallow and clear water conditions.

Previous exploration on sediment dynamics relate to equally flow structure and sediment load rates at confluence channels, including regions of bed scour and bar complexes below downstream junction corners in asymmetric planform led to an understanding of salient morphological features at confluences (Best and Rhoads, 2008; Boyer et al., 2006; Borghei and Jabbari Sahebari, 2010; Balouchi and Shafai Bejestan, 2012; Balouchi et al., 2015; Ghobadian and Shafai Bejestan, 2007; Leite Ribeiro et al., 2012a; Liu et al., 2012; Rhoads, 1996; Rhoads and Sukhodolov, 2001; Shafai Bejestan and Hemmati, 2008). Many features, such as high flow, intense turbulence, shear layer effects, and spiral circulation due to curvature, have been associated in causing scour hole formation. Experimental studies show that sediment loads inside a scour region become progressively dissociated through increasing discharge ratio and confluence angle (Best 1988). But, field investigations on the discordant confluence revealed that sediment transport rate occurred at the edge of the shear layer with sedimentation from the Pitraganj stream to the reverse bank of the major stream under excessive momentum ratio circumstances (Biron et al. al. 1993; Boyer et al. 2006). Balouchi and Shafa Bejestan (2012) examined the influence of live bed conditions on maximal scour depth at convergence channels and revealed that increasing bedload reduced the utmost scour depth ratio by as much as 35 percent. Balouchi et al. (2015) predicted maximum scouring depth at channel junctions under live bed circumstances using three different soft computing models viz. multi-layer perceptron (MLP), radial basis function (RBF) and M5P model tree. Model performance under live-bed situations showed that the MLP model had the highest level of accurracy in the small scour depth span, while the RBF model had a higher level of accuracy in the high scour depth range. Nargess et al. (2017) experimentally investigated local scour control at the convergence channel and found that the scour depth rely on the flow ratio, densimetric Froude number (Frg) and confluence angle. Leite Ribeiro et al. (2012a) examined the impact of branch channel with sediment feed to a major channel with excessive discharge. They showed that the three-dimensionality of the flow enhances the sediment transportation capacity at the lower channel and that turbulent kinetic energy is elevated close to the shear layer.

Field studies are becoming a progressively popular tool in the study of confluence because of the complexity involved in extrapolating laboratory results to real cases (Parsons et al. 2007). To a smaller extent, several field studies of channel morphology, sedimentology (Rhoads et al. 2008; Riley and Rhoads 2012) and particle tracing investigations have been conducted to comprehend sediment trajectories. Field surveys on sediment transportation and bed parttern at channel confluences supported that channel morphology is continually changing due to unstable sediment influx and sediment transport capacity. According to Sadeghi and Kheirfam (2015), sediment load behavior and channel bedform are determined by climatic and fluvial conditions. Moreover, the physical properties of bedload change under different temporal and hydrological circumstances, which greatly affects the accuracy of bed load model estimation (Sadeghi and Kheirfam, 2015; Monsalve et al., 2016; Wyss et al., 2016).

An unresolved problem is how the hydrological variabilityof contributory channels changes channel form and sedimentation at the confluences over time, and is a problem that needs to be addressed. The significance of bed load movement on the surficial pattern of bed materials at confluences are still largely unexplored. Bedload transport rate in confluences has been recognized as large spaces and prolific grounds for exploration. The results clearly demonstrate the need for research to analyze bedload behavior and its components under various circumstances.

In light of this, field investigations of morphodynamics have been conducted in the river confluence during the course of a short study period of one year (2018–2019) with various fluvial behaviour, with the following goal: (1) to evaluate the temporal fluctuation of bed load quantity and particle size; (2) to examine the effects of the flow-induced bottom oscillatory motion and unidirectional flows on bed morphology; and (3) to establish a relation between bedload transport dynamics in fluvial system and resulting bedform patterns. Therefore, these studies provide a detailed description of measurement of bedload transport, and demonstrate the short-term alterations in bed form and surface material in response to hydrologic variation in contributing rivers at a small asymmetric confluence in Tripura, India.

Materials And Methods

Description of the study site

The survey area is the confluence of the Gumti river (main channel) and the Pitragang river (branch channel or tributary), 56 km southwest of Agartala city, Tripura, India (Fig. 1). The Gumti watershed (2492 km² = 1921 km² belongs to the hilly terrain, only 571 km², about 23% of which is in the plains) is located in the lower-middle part of Tripura. It lies between latitude 23°47'N and latitude 23°47'N and longitude 91°14'E and longitude 91°58'E. The Gumti River is the largest river in Tripura and borders Bangladesh to the east and west. A few tributaries spread on both sides. The river elevation varies from 18.288 m to112.166 m above mean sea level and length is 167.4 km. Locations were selected based on three circumstances. First, the convergence needed to be a sandy-bed to increase the potential for progressive sediment movement and bed morphology occurrence with changing flow levels. Second, the widths of the merging canals were not equal, and the beds had to be of different heights. The width of the channel should be minimum to allow a thorough survey of the site immediately. Finally, the survey area had to be easily approachable to permit current and bed-loaded transport measurements anywhere within the convergence using motor boats or experimental boats. The Gumti-Pitra confluence met the above criteria well as it is a sandy confluence with confluence rivers of unequal width. The confluence narrows to 110 m wide at its apex and 85 m wide farther downstream. The tributary channel bed is about (Δz = 0.80 m) higher than that of the main river bed and meets the junction at an angle (θ) of 82 degrees. Here $\Delta \mathbf{z}$ is the bed level difference between the Pitraganj stream and the Gumti stream. Confluences have no vegetation effect. Both channels flowing together have different particle size distributions.

Figure 1

Hydrodynamics Characteristics Of The Confluence

In this study, the confluence can be defined as the union of two components: a deep region and a shallow region (Fig. 2). The local transport of sediment is significantly impacted by this separation. During floods, floating debris travels through the tributary to the confluence and gets trapped. During the study period, the tributary channel showed a fairly uniform cross-sectional flow with a mean velocity of $0.46\mathrm{to}0.78\mathrm{ms}^{-1}$and a flow rate of $14-46m^3s^{-1}$. In contrast, distribution of the velocity in the upstream parts of the Gumti river was very uneven, with fluctuations in velocity of $\left(0.56-1.02ms^{-1}\right)$ initiated due to the roughness of the bedform. The occurrence of bedforms and bed discordance lead to the formation of swirling flows on the surface, creating the characteristic of circular forms at the entrance of the tributary. Near the downstream of the CHZ a decrease in upwelling flow was observed, resulting in the deposition of fine suspended sand. Hydraulic characteristics of the confluence is presented in Table 1.

Table 1
Summarizes the dimensions measured and mean hydraulic characteristics of the river confluence between January 2018 and March 2019.

Channel	$W\,(m)$	$h\,(m)$	Q $\left(m^3/s\right)$	$\left(\bar{U}\right)$ (m/s)	S $\times10^{-3}$	W/h	M $=\rho Q\,\bar{U}$ $\left(Kgm/s^2\right)$	$Fr=\bar{U}/\sqrt{gD_h}$	Re $=\rho D_h\,\bar{U}/\mu$ $\times10^6$
Main (U/S)	75	1.52	88	0.77	0.58	49	67625	0.20	1.17
Main (D/S)	85	1.45	109	0.88	0.63	59	95728	0.23	1.28
Tributary	35	0.91	21	0.66	0.61	38	13846	0.22	0.60
Note: Vegetation presence (none)									

Here, W = width of channel (m), h = flow depth (m), Q= discharge in $\left(m^3s^{-1}\right)$, $\bar{U}$ = mean flow velocity $\left(ms^{-1}\right)$, ρ = water density $\left(Kgm^{-3}\right)$, μ = dynamic viscosity of water $\left(Kgm^{-1}s^{-1}\right)$, S = channel slope, D_h = the hydraulic depth (m), M= momentum flux $\left(Kgms^{-2}\right)$, Fr = Froude number of flow,Re = Reynolds number of flow, and W/h = aspect ratio.

Figure 2

Field Survey And Data Collection

A field survey was carried out through various hydrological seasons namely spring (March - May), summer (June - August), autumn (September - November) and winter (December - February) and extended from apex of study area junction to a length of 1500 m upstream in each of the two channels and 3000 m downstream. Surficial material samples were collected on thirty six (36) separate days between January 2018 and March 2019 in the upstream-downstream part of the confluence channel. During field campaigns, data were accompanied by hydrological data collection from upstream stage recorders and converted to flow rate using stage-discharge rating curves (Fig. 3**).** The rating curve is the relationship between stage (river water level) and streamflow (discharge). A rating curve was established, because at many channel locations the flow is not a specific function of stage; but slope of water surface, channel geometry, and unsteadiness of flow. So, the rating correlation established is thus used to convert the observed stages into the equivalent discharges. Field data is analyzed analytically and compared to stage record data. It is understood that during the six-day bathymetry survey of each campagain did not show any substantial variations in water levels and stream discharge. However, at the mouth of the tributary, a variation in water depths was observed according to high or low flow circumstances. Observations of stage fluctuations at three locations upstream, within the confluence and downstream were recorded every hour. The discharge of the converging channels is $Q_t \text{and} Q_m$. where$Q$is discharge $\left(m^3 s^{-1}\right)$ and subscripts $t$and $m$refer to the tributary and upstream of main river, respectively. The minimal and maximal flows recorded at downstream of the confluence are 48 and 212 $m^3 s^{-1}$ respectively. The flood season of the river occurred between June and September and the flow remained low in the river for the rest of the year. During the flood period, the flow of the rivers is more dominant than other periods. So, all the measurements are taken after the flood recedes. The wind speeds were collected from the closest radar station established by Indian Metrological Department (IMD) and ranged from 18 knots to 32 knots (1 knot = 1.852 km/hr). Measurements of bedload transport rate were performed using a Helly-Smith (HS) bedload sampler at three different points on each section and done at different stations. Depending on the rivers flow and the characteristics of the sediment, a sampler was lowered to the river depth for each bedload measurement. In deep region, the measurements are repeated many times before reliable results are obtained. Optimal sampling times were found to be in the range of 15–30 minutes. This will avoid the bag being about 50% full. Since the HS spun round in the recirculation region next to the inner bank, no sampling could be acquired and only measurements of water depth were taken. A total of 432 samples were collected during the whole fieldwork, but hazardous flow situations prevented data collection in just a few days. Bed load transport rates are calculated using direct and empirical methods. A bathymetric survey of confluence river was performed with a Single Beam Echo Sounder (SBES) operating at 20 KHz and deployed from a small boat. In addition, a high-speed digital camera was used to detect sand ripples, and automated levels and river staff gauges were used to determine the bed height of each section as well. A video method was used to generate statistics on the presence and composition of sand ripples. In this work, a Nikon Digital camera was utilised to capture the river bed images (bedforms). The camera was lowered to 0.5 meters above the riverbed with a fiberglass core to allow real-time video transmission. The position of the camera system in the riverbed was controlled by manually adjusting the cable length based on the video feed live from the winch. Video recording were performed within an hour time frame in relatively calm weather conditions. The camera continuously recorded images of the riverbed, and video images (frames) were automatically created from these footages every second. All selected video images were analyzed using Image processing software, ImageJ 1.51n (Schneider et al., 2012).

Soil samples were taken from the channels and examined as illustrated below to define the PSD for each channel. Sampling points were chosen in the immediate vicinity of the running water, and samples of 50–80 kg of subsurface material were taken once at the same point, allowing for compatible assessment of the spatial form of the material features between sampling days. The collected materials were dried at room temperature and lightly granulated for sieve analysis. Sieve analysis was performed in the laboratory using an electric sieve shaker to test samples from 0.075mm to 2mm. Sieve analysis was followed by hydrometer analysis on 50-gram soil samples finer than 0.075 mm to workout the classification of finer grain particles. This fraction was mixed with 20 ml of sodium hexametaphosphate solution and 200 ml of distilled water for 30 minutes and placed in a shaker. For the purpose of performing hydrometer analysis, 800 ml of fresh water was added and the mixture was kept in a steady temperature bath for 48 hours.

Figure 3

Bed Material (Grain Size)

Particle size distribution (PSD) plots and sediment properties of the samples identified in Fig. 4 confirm the sieve analysis results in Tables (2 and 3). Particle size distributions provide an important information on sediment motion and accumulation to understand the hydrodynamic properties of the respective sediment areas and relates sedimentation processes (Zhang et al. al. 2015). During this study, the riverbed at the Gumti confluence is composed of sandy material, so the sediment density for the entire model is set to the default value of 2650kg/m^3.

Table 2
displays the percentage of sediment size of collected samples obtained from PSD analysis during the period (2018 and 2019).

Samples Locations		**Sand (%)** $1-2mm$	**Sand (%)** $<1mm$	**Silt (%)** $0.002-0.05$	**Clay (%)** <0.002	**Total**
Gumti River		11.34	83.75	3.28	1.63	100
Tributary		6.72	87.46	4.77	1.05	100
Confluence	Shallow	10.76	41.67	2.72	1.31	56.46
	Deep	14.59	24.54	1.37	3.04	43.54

Table 3
shows the mean characteristics of the sediments collected over a period of time (2018 and 2019)

Channel		d_{16}	d_{50}	d_{84}	σ	$\varphi\,(deg)$	θ_{cr}	Re_*	d_*
Main (u/s)		0.35	0.53	1.1	1.78	28.6	0.032	98	21.17
Tributary		0.28	0.46	0.89	1.78	31.2	0.03	67	18.37
Confluence*	Shallow	0.25	0.39	0.65	1.61	32.4	0.03	69	14.58
	Deep	0.22	0.34	0.54	1.57	34.1			

*Taking mean value of deep and shallow area for$\theta_{cr}, Re_*and d_*$

Here, σ is the geometric standard deviations of the PSD $(=\sqrt{d_{84}/d_{16}})$, where d_{16} and $d_{84}$are the particle sizes finer than 16 and 84% by weight respectively, φ is the angle of repose of river sand, $Re_*$is particle shear Reynolds number $(=u_*d/\nu)$, here $d=d_{50}$ is grain size, ν is the kinematic viscosity of the fluid, and θ_{cr} is the critical value of Shields parameter for the incipient sediment motion, and is estimated using the relationship proposed by Soulsby (1997).

$$\theta_{cr}=\frac{0.3}{1+1.2d_*}+0.055\left[1-exp\left(-0.02d_*\right)\right] (1)$$

where, d_* is dimensionless particle size given as:

$$d_*=\left(gR/\nu\right)^{\frac{1}{3}}$$

2

where R is the specific weight of submerged particle (R = 1.65).

Figure 4

Direct Method

The direct method was applied in the bathymetric survey to calculate the bedload transport rate. A Helly-Smith sampler was employed to collect the sediment sample volume, thus enabling direct assessment of bedload movement. Therefore, the unit bedload transport

rate is estimated as (Van Rijn, L.C 1986, 2007):

$$q_b = k\rho_s (1-p) \times (V/bT)$$

3

in which, $k$is the calibration factor $(= 0.5)$ for particles in the range $0.25 - 0.55$ mm,ρ_s is the volumetric mass of sediment particles (= 2650 Kg/m^3), $p$is the porosity factor $(0.4 - 0.6)$,V is the immersed volume of sediment catch (m^3), $b$is width of intake opening (= 0.0762 m), and Tissampling period (s). All unit bedload flow rates were then united over the transect to calculate the total bedload discharge according to Eq. (4).

$$Q_b = \sum q_{bi} W_i$$

4

where $Q_b$is the total bedload discharge (Kg.s^{-1}), $q_{bi}$is the unit bedload rate on a vertical $(Kg/m.\,s)$and W_i the width of the subsection (m). Twelve bedload measurements were made in one day owing to various outcomes of the actual bedload from deep and shallow areas. The bedload transportation rates quantified by the sampler range from 0.6 to 1.25 Kg. s^{-1} and was computed for an entire 36 days for flows in the range $48 - 212 m^3/s$ and compared with the Van Rijn empirical method.

Empirical Formula

There are several bed load equations developed and supported various theoretical concepts such as shear stress, stream power, probability, and dimensional equality etc. Additionally, conceptual equations, empirical equations supported the laboratory experiments, and field measurements have been proposed by various researchers. The applicability and suitability of the equations vary from case to case, and therefore the uncertainty of the dynamic combination of parameters involved in bed load transport, sometimes necessitates adjusting the equation chosen based on field observation. In the current analysis, Van Rijn (1993) equation is applied to evaluate the transport rate of bedload by acquiring various characteristic sediment sizes in the PSD of the sample.

The one-dimensional and a nonlinear bedload transport formula with particle sizes in the $0.2 - 2\mathrm{mm}$range developed by Van Rijn (1993) corresponds to the mean particle dimension of the surficial material, d_{50}in the bed. The bedload discharge computed from the VR,equation, $(q_b)_{VR}\left(Kgs^{-1}.m^{-1}\right)$, is calculated as:

$$(q_b)_{VR} = 0.053 T^{2.1} \frac{[(s-1)\,g]^{0.5} (d_{50})^{1.5}}{d_*^{0.3}} (5)$$

where $s$is the sediment density ratio (2.65); $g$is the gravitational acceleration; $d_{50}$is the mean particle dimension of the surficial bed material; and T is the transport stage shear parameter, and is computed using the subsequent formula:

$$T = \frac{(u'_*)^2 - (u_{*cr})^2}{(u_{*cr})^2} (6)$$

Where u'_* is the effective shear velocity related to bed grains and u_{*cr} is the critical bed shear velocity expressed as:

$$u_{*cr} = \left[0.013 d_*^{0.29} (s-1)\, g d_{50}\right]^{0.5} (7)$$

VR method was applied to 432 data sets to calculate the unit bedload transport rate that were obtained between low discharge $\left(48 m^3.s^{-1}\right)$ and peak discharge$\left(212 m^3.s^{-1}\right)$. Total bedload measured by HS sampler is 4.4 tons and and 9.92 tons in tributary and main channels, respectively in thirty six (36) days. On the other hand, the total bed loads calculated by the VR method are 5.2 tons and 10.98 tons in tributary and main channels, respectively. Average shallow region unit bed load q_b ranges from 0.028 to 0.056 Kg/s, whereas in deep region average unit bedload q_b ranges from 0.015 to 0.032 Kg/s. At all transport stages, the bedload rate predicted by the Eq. 3 is the flow rate measured by the sampler. Bedload transport velocity exceeded 1.89 Kg/s in the branch channels when flow was predominant. Over the whole study period, the minimum daily bedload volume achieved in April in the main channel was only 38

kg/day, while the maximum daily bedload volume recorded in October was 80 kg/day. Therefore, the ratio of minimum and maximum transportation rate in the major and branch channels is 0.48 and 022 respectively. It was discovered that transport rate of bed load was more in shallow area than in deep water. This is mainly due to the combine effect of wind and current, and the bed stress caused by the frictional force of flowing water and the action of tributary caused by sediment inflow is more in shallow regions than in deep regions. Under low flow conditions in summer, the bed load of fine-grained sediments was the highest. In autumn and early winter, medium-grained sediment transport was higher, which corresponded to the occurrence of extreme rains and floods. Bedload like the 70 m wide shallow region accounts for 64% of the total volume, and therefore the outstanding 36% corresponds to the 40 m wide deep region are not the same as those carried by the tributary channel and the major channel, respectively. A comparison study of unit bedload rate computed from empirical and field measured data is presented in Fig. 5

Figure 5

Results

Observations of channel morphology

This section reports the short-term fluctuation in the textures of surficial material and channel morphology associated with varying flow conditions between January 2018 and March 2019. Conditions in monsoon reflected the continual consequences of large discharge flows since summer. These continuous flows created a sand-laden bar structure at downstream junction corner adjacent to the inner bank, progressively slowing the main river flow (Fig. 6). Most changes in post confluence channel along the inner banks are due to complex sedimentation and erosion driven by short-term hydrological fluctuations. The presence of bar structure redirect flow to the middle of the lower confluence and protect the inner bank from erosive forces. At high flow rate, the flow turns progressively to the outside bank as it passes the junction and enters the lower confluence channel, leading to a wide bar pattern nearby the inner bank and create a minor scour pit next to the outside riverbank (Fig. 7). On the other hand, low flow cause significant erosion of the bar pattern and begins to realign the scour hole around the middle part of the postconfluence channel. Over time, main bar and a fine-grained minor bar accumulated at the lower end of the main bar together to form a complex bar structure next to inner bank, and the region where the minor bars were previously situated (cross section C), is underlain by sandy material. The deposition of fine materials in the developing bar structure, which emerges as a sediment wedge from the tributary, increases the bed elevation by 0.24 m within the confluence and increases the flow separation adjacent to the bar structure (cross sections A, Fig. 6). The bar structure projected into the junction and subsequently extended along the inner bank, resulting in usually asymmetrical river profiles at the investigated transects (A, B, and C) (Fig. 6). The cross sectional profiles in the confluence was almost regular (transect A), as the bar pattern from the tributary virtually prolonged the whole width of the confluence. Surficial sediment mainly consists of fine sand extending along the surface of the bar form (Fig. 6). The surface of the bar was slightly eroded and the scouring holes were restricted to the outside bank at the base of the projecting portion of tributary deposit. Channel asymmetry improved across the downstream transect as scouring depth expanded through the outer bank and bed materials accumulated across the inner bank. These results are somewhat different from those of experimental investigations of asymmetrical confluences, that reported the scour holes were aligned with dominant tributary (Best, 1988).

During a prolonged period of changing hydrological circumstances from early July to mid-October, the total flow at the confluence magnified significantly compared to the spring (March-May) and early summer (June-August) flows. Significant channel adjustment was made by a short-term change in fluvial circumstances. Approximately 0.26 m to 0.34 m of sedimentation was detected on the edge of inner bank of the lower confluence channel from July to October. However, the previously projecting sediment wedge eroded from the tributary channel, resulting in a bed elevation reduction of 0.15–0.32 m and a displacement of this sediment wedge 1.75–2.85 m towards the inner bank. Channel morphology and patterns of bed sediments on this month largely reflect persistent high flow conditions. The spatial structure of bottom sediments after low-flow events is different compared to high-flow situations. This is because the sediment inputs from the branch channel and the main stream are still clearly separated far below the confluence. Between surveys, the bed elevation in the middle of the receiving channel changes, demonstrating dynamic adjustment to fluctuating flow conditions. The channel profile is nearly symmetrical on all cross-sections except for the most downstream location. Channel irregularities further downstream than section C were less pronounced than in July and October. This is because fine-grained secondary bars that were existing in spring and early summer were removed by shallow flow rates in January and March and were not rebuilt in the side of the primary bar. Comparing the channel cross-section surveys, it is seen that the spatial distribution of bed

materials and bedform in July and October are similar, although there are some differences. Significant hydrological processes under high flow circumstances that maintain the present morphological structure of the bed.

Fine materials that were existing on the outer bank exactly lower end of the junction corner in January 2018 have not spread as far downstream as they did in July and October 2018. Surface material distributions in April 2018 and March 2019 show definite regions of mixed sand and fine sediments within the confluence. However, at the confluence (cross section A), fine sandy sediments are found next to the inner bank, extending inwards to the middle of the lower confluence stream. This bed pattern corresponds to a typical confluence sediment transport pattern in low flow situations.

Figure 6

Figure 7

Ripple Geometry Under Combined Flows

Fundamentally, understanding the profile of ripple is essential for calculating sediment transport in stream and coastal regions. Fieldwork was done at the Gumti confluence to examine bedform dynamics under various hydrodynamic and hydrological circumstances connected to flow and wind-induced flow. In the current study, a survey was conducted at low water level under various driving situations to collect comprehensive data on ripple geometries. In order to compile data on the distribution and presence of sand ripples, video techniques were used. The typical two-dimensional ripple cross-section geometries with straight crestlines captured in the relatively mild and temperate weather conditions during field survey are shown in Fig. 8. A plan view of the ripple cross sections was acquired from different environments, with each area approximately $900cm^2$ $(30cm \times 30cm)$ cropped from the specified measurement area $3m^2$ $\left(2m^2 \times 1.5m^2\right)$. The cross-sectional profile of the ripples revealed an asymmetric shape with the ripples aligned in the direction of the flow current (Fig. 9). Bed topography studies have shown that mixed sand dominates the bed sediment in the HCZ and the ripple trains are two-dimensional with highly straight crest line. A comparative analysis shows that, with very minor alterations, the morphology of the riverbed is essentially the same from July – October, 2018 and on January 2018, 2019 (Fig. 8).

Previous investigations have shown that flow parameters and sediment characteristics significantly influence ripple geometry (e.g., Allen, 1984; Southard, 1991). However, the current results indicate that the riverbed configurations may be more sensitive to combine flow than the single-channel flow documented in the literature or by many researchers previously. The current study found that precise ripple geometries can be provided under combine flow circumstances. The extent of ripples for statistics was calculated and the overview of ripple-geometry characteristics is shown in Table 4. Fieldwork showed that the average ripple length and elevation were 85.5 mm and 3.8 mm, respectively. It was found that the Ripple Symmetry Index, RSI (ratio of stoss side to lee side length; Dumas et al., 2005) $(> 80\%)$, to be greater than 1.35. This indicates that ripples commonly generated during the study period are asymmetric, with a maximum RSI of 1.51. The statistical solution of ripple cross-sectional shapes show that Ripple Index, RI (ratio of ripple length to elevation; Dumas et al., 2005), values are varying between 10 and 85. In accordance with field surveying, the most of ripples were affected by current flow and moderate wind speeds (50–60 Kmph), with the majority of ripples exhibiting a shorter ripple length on leeward side than the stoss side.

The current field observations show that modest wind speeds dominant and are enough to produce transitions between the bedform states of lower regime and bedform phase morphological spaces. Therefore, it is possible that the mild wind caused a bottom oscillatory motion that significantly altered the bed morphology. Moreover, in moderate to moderate wind conditions and in the presence of mixed flows, the bed pattern can evolve from a 2D asymmetric ripple to a 2D symmetric wash-out ripple to a flat bed. According to frequency curves of ripple size, most of ripple elevations (η) ranged between 5 mm and 9 mm, and ripple lengths (λ) ranged from 75 mm to 85 mm (Fig. 10). The RI frequency curve peaked at 20. Additionally, the majority of the RSI is between 2.25 and 5.85. This demonstrates that during the study time, these ripples were the most asymmetrically produced. Geometries of the ripple cross-sections analyzed statistically reveal that the RSI exceeded 1.24 and peaked at 1.59. As a result of the field survey, it became clear that ripples with continuous straight crestlines are typical. However, the separate ripple geometries were significantly different from those measured in January 2018. In fine-grained sediments, both plane beds and wash-out ripples typically occur at comparably large bed shear stress (Allen, 1984; Van Rijn, 1993; Leeder, 2011). A complete change in ripple shape was observed after a moderate wind blow. The plan view represents that the ripples are being substantially flatter, due to the average ripple length increased slightly to 71 mm and the average ripple height decreased significantly by 3.5 mm. The ripple index increased dramatically compared to the 2D ripples observed in January 2018, with an average RI of 85 (Table 4).

Table 4
Outline of ripple-geometric properties

Round	Date	λ (mm)	$\lambda\sigma$ (mm)	η (mm)	$\eta\sigma$ (mm)	λ_s (mm)	$\lambda_s\sigma$ (mm)	λ_l (mm)	$\lambda_l\sigma$ (mm)	RI	$RI\sigma$	RSI	$RSI\sigma$
1	25/01/2018	75.8	13.19	0.89	0.38	38.66	10.37	28.14	9.0	85.16	24.61	1.37	0.48
2	20/04/2018	84.6	14.30	7.82	2.42	36.68	9.04	26.75	7.07	10.82	3.28	1.37	0.32
3	14/07/2018	78.5	13.66	8.12	2.44	41.28	9.53	33.42	9.95	9.67	4.15	1.24	0.44
4	24/10/2018	68.5	12.65	2.78	0.89	35.69	8.81	26.28	6.95	24.64	13.41	1.36	0.32
5	16/01/2019	55.6	8.84	0.65	0.29	31.42	9.42	20.87	6.79	85.54	24.78	1.51	0.50
6	22/03/2019	62.5	9.97	0.68	0.31	33.57	7.10	21.15	4.45	91.92	26.56	1.59	0.66

Here, λ is the Ripple length; η is the Ripple elevation; λ_s is the Stoss side length of ripple; λ_l is the Lee side length of ripple; and σ is the Standard deviation.

Figure 8

Figure 9

Figure 10

Equilibrium Between Main River And Tributary

Considering the position of the transect, it is clear that the bedload in the shallow and deep regions are distinctly different, with the loads contributed by the branch channel and mainstream, respectively. The bedloads are not fully captured by the HS measurements in the deep area. Recall that at the confluence mainstream ruptured the deep region bed by 0.8 meters to better support the sediment supply. On the other hand, a long imaginary boundary that separates the shallow and deep discordant zones stretches 100 m upstream of the transcent. The bed discordance was overcome by bedload of nearby confluence passing through the deeper parts to reach the bar. Because it contributes to the dynamics of the bars, sorting in the separation area can cause more sand to flow over the shallows. The inward near-bottom flow, which drags the bed particles exactly toward the shallow region as part of the spiral flow, must match the outward near-surface flow (Rhoads and Kenworthy, 1995; Best and Rhoads, 2008). However, this may be more noticeable downstream of transects where scour holes are the deepest. Mainstreams behave more non-linearly and appear to have significant amounts of bedload at higher flows, while tributaries seem to yield more bedloads on average. The sand content in the shallow and deep part is 25 and 14 percent of the total amount, respectively. Although it is not quantified, there is on doubt that fine sand gets mixed into the suspension as load hits the deep area. This imbalance can be explained by the growth of unmeasured suspended means of transportation when the sediment load enters the lower area.

Discussion

Observations of channel morphology

Results from short-term analyses of morphological changes indicate that erosion and sedimentation patterns in the confluence are extremely susceptible to hydrological changeability. A continuous flow creates and maintains a wide bar structure in the inner bank and forms a thin scour pit on the outer bank. Low-flow events cause scouring to move toward the middle of confluence area and materials deposit on the outside bank, creating a symmetric transverse-channel profile in the postconfluence channel. The spatial pattern of material responds to changes in flow conditions that facilitate material intrusion from branch channel over confluences into lower channels. Sediments entering the confluence from the both main and branch channels travel laterally through the lower channel from the outside bank to the edge of bar adjacent to confluence corner. Surficial bed material with distinctively PSD results from the merging of the sediment loads in the lower channel reflects the dominant pattern of sediment movement through confluences and is compatible with the spatial pattern of sediment under low-flow circumstances. However, Best and Rhoads (2008) found that within the

CHZ, erosion and sedimentation patterns reflected alterations in bed shear stress in response to changing from low-flow to high-flow characteristics, which creates distinction in bedload transport capacity and leads to variations in bed form during particular fluvial circumstances. When there is a high flow rate, flow curvature from tributaries to downstream channels has two effects that affect surface material and bed morphology. Prior to sedimentation on the inner bank and subsequent refinement of the particles on the bar surface, the level of the bed stress around the inner bank rapidly reduces, analogous to the pattern in meander bend (Dietrich, 1987). A region of maximum bed stress nearby the middle of the channel excavates the sediments deposited in the inner part of the channel downstream, developing a comparatively symmetrical transects profile. Second, the streamline curvature causes the downstream channel to generate helical flow distinguished by outward flow close to the surface and inward flow at the bed (Rhoads and Kenworthy, 1995). The inward flow at the bed along the outside bank washes fine grain from the main channel to the inner wall, and promotes mixing of fine- and medium-grained sediments receiving from the two converging channels in the downstream channel.

Rhoads (1996) reported that two surface-convergence spiral cells developed on both side of the MI at the mouth of tributry to the lower channel, assisting in the scour and separation of sediment loads by washing sediments laterally from the centre of the CHZ. Materials from the two converging channels are forced to the opposite sides of the scour pit within the junction, prior to merge into the lower channel. The secondary circulation pattern changing from two surface-convergence cells to one dominant helical cell has an impact on this coalescence because it causes the bedload to simultaneously move from the inner wall to the outside of the lower channel.

Results from a short-term investigation on the relationship between bed morphology and hydrological variability indicate that high flows promote sedimentation along the inside and scour at the toe of the outside bank. Short-term analyzes indicate that low flows do not encourage significant recovery of high-flow effects by depositing grain particles along the outer bank of lower channel. This overall net change in confluence morphology was modest, in contrast to the huge changes that can happen in unconstrained junctions such as braided rivers (Ashmore and Gardner 2008).

Ripple Geometry Under Combined Flows

Past studies have presented that understanding of ripple shape is fundamental for calculating sediment movement in the river and coastal zone, and is strongly influenced by stream discharge and sediment properties (e.g., Allen, 1984; Southard, 1991). Previous studies have shown that effect of storm produced strong oscillatory motion can alter morphodynamics, promoting undulating ripples and sediment transportation (e.g., Passchier and Kleinhans, 2005; Aagaard et al., 2012). Though, current field survey review that medium winds are strong enough in the bedform phase space to form a transition to the upper regime bedform state. Under these situations, the consequences specify that the combination of current flow and wind generated flow produces enough bed stress to modify the transport approach.

The present study suggests that, bed geometries may be more responsive to combined flows than earlier speculation. These results confirm earlier research (Grant and Madsen, 1979) and imply that the presence of wind currents increases the induced bottom shear stress. In other words, the configuration of the river bed evolves from a 2D asymmetric ripple to a 2D symmetric washed-out ripple, from calm to moderate circumstances to a flat bed with combined flow. Field observations highlight that most ripples are modified by the combined action of wind and flow under prevailing conditions, with most ripples having downwind wavelengths shorter than their impact side lengths.

Given the significance of bed pattern in response to irregularity of stream discharge and mode of sediment movement, further investigation on morpho-dynamics are needed under various associated flow circumstances. This is crucial for making it possible to enhance the hydrodynamic and sediment transport models for river network systems that are currently in use. Future study in this field will focus on developing a thorough understanding and extensive knowledge of the interactions concerning flowdynamics, turbulence dynamics, and sediment transport under severe meteorological conditions.

Balance Between Main River And Tributary

A shallow zone towards the inner and a deeper zone towards the outer constitute the confluence region. Across the hypothetical boundary between these two regions, some of the incoming load from the pitragang tributary is transported into the deeper zone. In the present study, two different bedloads at the transect are observed. One kind of tributary bedload crosses the transect directly along the shallow region, whereas another kind crosses the transect indirectly along the deep region subsequently entering the deeper part of the

junction. Although the kinds of indirect transport are inadequate to satisfy the capacity of deep zone transport, but the kinds of direct transport are basically at its capacity. According to Boyer et al. (2006), the largest transfer rates happen close to the shear layer edges where the two confluence converge. Here, the bedload distribution was vary as a result of shifts in the shear layer caused by variations in discharge in two confluence channel, especially when the flow in the main stream (Gumti River) is predominant and the shear layer is moved to the inside. As a result, the swirling area without transport is located to the outside of the shear layer border. Figures 6 and 7 represent only a mean of the many circumstances. Best and Rhoads (2008) point out that the scour pit at the junction prevent intrusion of debris bedload flowing through the flanks. In that instance, active involvement of the tributary pushed into the scour hole on the outside and supplied majority of the bedload.

Conclusions

This study explored how a tributary channel affected the structures of surficial material and the morphology of the downstream channel close to the confluence. Towards this attempt, field investigations were carried out near the river confluence as part of this effort from January 2018 to March 2019 to evaluate the temporal change of bed load volume and features under various hydrological circumstances. To find sand ripples, a high-speed digital camera was employed, and video techniques were used to produce statistics on the geometry of the ripples. As reported by the study, the Gumti-Pitragang river confluence caused a area of stagnation in the upstream corner of the junction that had led to the formation of shear layers and a region of deflection. Before merging in the downstream channel, approaching sediment loads are separated about the core area of scour. It is clearly understood from the observation data that high discharge flows result in a wide bar structure close to the downstream junction corner and a contracted scour hole beside the outer bank. Low flow rates cause significant erosion of the barform at the side of inner bank and realign the scour pit near the confluence zone and the middle of the lower channel. The consequences indicated that in the course of the floods and sand extraction seasons (rainy season), the bed load transportation increased considerably. A combined effect between increased the flow rate and the intensity of sand extraction has increased the transportation of the bedload. The fine-grained sediments had an abundant bed load in low flow circumstances and over the summer. Due to heavy rains and flooding in autumn and early winter, the transport of medium-grained sediments has increased. The current study showed that at asymmetrical stream confluences, short-term hydrological variability can have a considerable impact on the morphodynamics of the river bed.

As the sampler efficiency declines for coarse-grained material, the assessment of bedload across the deep region is less precise. In terms of average bedload quantities, the confluence is perhaps imbalanced on the side of the tributary. Under calm environment, 2D ripples with straight peaklines were detected and were asymmetric with an average RSI of 1.4. Most of the ripple heights ranged from 5 mm to 9 mm, and lengths ranged from 75 mm to 85 mm. The shape of the ripples was dramatically altered by flow-induced near bed flow oscillation, and produced the 2D regular washed-out ripples after a period of severe winds. Moreover, after strong winds, plane beds emerge. Given the significance of river bed geometries in relation to bed texture and sediment transport mechanism, more research on morphodynamics in the extent of mixed flow situations is required.

Declarations

Acknowledgement

The authors acknowledge the financial support of Science and Engineering Research Board (SERB), Ministry of Science and Technology, Government of India (Grant No. EMR/2016/005371).

Conflict of interest The authors declare no conflict of interest in this paper.

References

1. Aagaard, T., Hughes, M., Baldock, T., Greenwood, B., Kroon, A., and Power, H. (2012) Sediment transport processes and morphodynamics on a reflective beach under storm and non-storm conditions. Marine Geology, 326–328, 154–165.
2. Allen J (1984) Development in Sedimentology 30: Sedimentary Structures their Character and Physical Basis. Elsevier
3. Ashmore P, Gardner JT (2008) Unconfifined conflfluences in braided rivers. River Conflfluences, Tributaries and the Fluvial Network. John Wiley and Sons, Chichester, pp. 119–147.

4. Balouchi B, Shafai Bejestan M (2012) The effect of bed load on maximum scour depth at river confluence. Journal of Ecology Environmental & Conservation, 18(1), 157–164.
5. Balouchi B, Nikoo MR, Adamowski J (2015) Development of expert systems for the prediction of scour depth under live-bed conditions at river confluences: Application of ANNs and the M5P model tree. Applied Soft Computing, 34, 51–59, http://dx.doi.org/10.1016/j.asoc.2015.04.040.
6. Best, J.L., 1987. Flow dynamics at river channel conflfluences: implications for sediment transport and bed morphology. In: Ethridge, F.G., Flores, R.M., Harvey, M.D. (Eds.), Recent Developments in Fluvial Sedimentology: Society of Economic Paleontologists and Mineralogists Special Publication No. 39. Society for Sedimentary Geology, Tulsa, OK, pp. 27–35.
7. Best JL (1988) Sediment transport and bed morphology at river channel confluences. Sedimentology 35: 481–498.
8. Best JL, Rhoads BL (2008) Sediment transport, bed morphology and the sedimentology of river channel confluences. In: Rice, S.P., Roy, A.G., Rhoads, B.L. (Eds.), River Confluences, Tributaries and the Fluvial Network. John Wiley and Sons, Chichester, UK, 45–72
9. Biron P, Roy AG, Best JL, Boyer CJ (1993) Bed morphology and sedimentology at the confluence of unequal depth channels. Geomorphology 8: 115–129
10. Biron P, Best JL, Roy AG (1996) Effects of bed discordance on flow dynamics at open channel confluences. Journal of Hydraulic Engineering 122 (12): 676–682
11. Biron PM, Richer A, Kirkbride AD, Roy AG, Han S (2002), Spatial patterns of water surface topography at a river confluence, Earth Surf. Processes Landforms, 27, 913–928, doi:10.1002/esp.359
12. Biron, PM, Lane SN (2008), Modelling hydraulics and sediment transport at river confluences, in River Confluences, Tributaries and the Fluvial Network, edited by S. P. Rice, A. G. Roy, and B. L. Rhoads, pp. 17–43, John Wiley.
13. Borghei SM, Jabbari Sahebari A (2010) Local scour at open channel junctions. Journal of Hydraulic Research, 48(4), 538–542.
14. Boyer C, Roy AG, Best JL (2006) Dynamics of a river channel confluence with discordant beds: flow turbulence, bed load sediment transport, and bed morphology. Journal of Geophysical Research 111: F04007. doi:10.1029/2005JF000458
15. Bradbrook, K.F., Lane, S.N., Richards, K.S., 2000. Numerical simulation of threedimensional time-averaged flflow structure at river channel conflfluences. Water Resources Research 36 (9), 2731–2746.
16. Bradbrook KF, Lane SN, Richards KS, Biron PM, Roy AG (2001) Role of bed discordance at asymmetrical river confluences. Journal of Hydraulic Engineering 127 (5): 351–368
17. Canelas OB, Ferreira R, Guillen-Ludeia S, Alegria F, Cardoso A (2020) Three-dimensional flow structure at fixed 70° open-channel confluence with bed discordance. J Hydraul Res 58(3): 434–446, https://doi.org/10.1080/00221686.2019.1596988
18. De Serres B, Roy AG, Biron PM, Best JL (1999) Three-dimensional structure of flow at a confluence of river channels with discordant beds. Geomorphology 26 (4): 313–335
19. Dietrich WE (1987). Mechanics of flow and sediment transport in river bends. In: Richards, K.S. (Ed.), River Channels Form and Process. Basil Blackwell, Oxford, UK, 179–224
20. Dumas S, Arnott R, Southard JB (2005) Experiments on oscillatory-flow and combinedflow bed forms: implications for interpreting parts of the shallow-marine sedimentary record. J. Sediment. Res. 75 (3): 501–513
21. Ghobadian R, Shafai Bejestan M (2007) Investigation of sediment patterns at river confluence. Journal of Applied Sciences, *7*(10), 1372–1380.
22. Grant WD, Madsen OS (1979) Combined wave and current interaction with a rough bottom. J. Geophys. Res., 84 (C4), 1797–1808
23. Leeder MR (2011) Sedimentology and Sedimentary Basins: From Turbulence to Tectonics. John Wiley & Sons, U.K
24. Leite Ribeiro M, Blanckaert K, Roy AG, Schleiss J (2012a) Flow and sediment dynamics in channel confluences. Journal of Geophysical Research, 117, F01035, DOI: 10.1029/2011JF002171.
25. Liu TH, Chen L, Fan, BL (2012) Experimental study on flow pattern and sediment transportation at a 90° open-channel confluence. International Journal of Sediment Research, *27*, 178–187
26. Monsalve A, Yager EM, Turowski JM, Rickenmann D (2016) A probabilistic formulation of bed load transport to include spatial variability of flow and surface grain size distributions. Water Resour. Res. 52, 3579–3598
27. Nargess Amini, Behnam Balouchi, Mahmood Shafai Bejestan (2017) Reduction of local scour at river confluences using a collar, International Journal of Sediment Research, 32 (3), 364–372, https://doi.org/10.1016/j.ijsrc.2017.06.001.

28. Parsons DR, Best JL, Lane SN, Orfeo O, Hardy RJ, Kostaschuk R (2007) Form roughness and the absence of secondary flow in a large confluence-diffluence, Rio Paraná, Argentina, Earth Surf. Processes Landforms, 32, 155–162, doi:10.1002/esp.1457.
29. Passchier S, Kleinhans M (2005) Observations of sand waves, megaripples, and hummocks in the dutch coastal area and their relation to currents and combined flow conditions, J. Geophys. Res. Earth Surf. (2005), p. 110
30. Rhoads BL (1996) Mean structure of transport-effective flows at an asymmetrical confluence when the main stream is dominant. In: Ashworth, P., Bennett, S.J., Best, J.L., McLelland, S. (Eds.), Coherent Flow Structures in Open Channels. John Wiley & Sons Ltd., Chichester, UK: 491–517
31. Rhoads BL, Kenworthy ST (1995) Flow structure at an asymmetrical stream confluence. Geomorphology 11: 273–293
32. Rhoads BL, Kenworthy ST (1998) Time-averaged flow structure in the central region of a stream confluence. Earth Surf. Process. Landf. 23 (2), 171–191. http://dx.doi.org/10.1002/(SICI)1096-9837(199802)23:2b171:AID-ESP842N3.0.CO; 2-T
33. Rhoads BL, Sukhodolov AN (2001) Field investigation of three-dimensional flow structure at stream confluences: 1. Thermal mixing and time-averaged velocities. Water Resources Research 37: 2393–2410
34. Rhoads BL, Sukhodolov AN (2004) Spatial and temporal structure of shear layer turbulence at a stream confluence. Water Resources Research 40: W06304. doi:10.1029/2003WR002811
35. Rhoads BL, Sukhodolov, AN (2008) Lateral momentum flux and the spatial evolution of flow within a confluence mixing interface. Water Resources Research 44: W08440. doi:10.1029/2007WR006634
36. Rhoads BL, Riley JD, Mayer DR(2009), Response of bed morphology and bed material texture to hydrological conditions at an asymmetrical stream confluence, Geomorphology, 109, 161–173, doi:10.1016/j. geomorph.2009.02.029
37. Riley JD, Rhoads, BL (2012) Flow structure and channel morphology at a natural confluent meander bend. Geomorphology 163–164, 84–98. http://dx.doi.org/10.1016/j. geomorph.2011.06.011
38. Roy AG, Bergeron N (1990) Flow and particle paths in a natural river confluence with coarse bed material. Geomorphology 3: 99–112
39. Sadeghi SHR, Kheirfam H (2015) Temporal variation of bed load to suspended load ratio in Kojour River, Iran. Clean- Soil, Air, Water 43 (10), 1366–1374
40. Schneider, C. A., Rasband, W. S., & Eliceiri, K. W. (2012). NIH image to ImageJ: 25 years of image analysis. Nature Methods, 9(7), 671–675. https://doi.org/10.1038/nmeth.2089
41. Shafai Bejestan M, Hemmati M (2008) Scour depth at river confluence of unequal bed level. Journal of Applied Sciences, *8*(9), 1766–1770.
42. Soulsby R (1997) Dynamics of Marine Sands: A Manual for Practical Applications. Thomas Telford
43. Southard, J.B., 1991. Experimental determination of bed-form stability. Annu. Rev. Earth Planet. Sci. 19, 423–455
44. Sukhodolov AN, Julian Krick, Sukhodolova TA, Zhengyang Cheng, Rhoads BL, Constantinescu GS (2017) Turbulent flow structure at a discordant river confluence: Asymmetric jet dynamics with implications for channel morphology. JGR Earth Surface 122 (6): 1278–1293
45. Van Rijn LC (1986) Manual sediment transport measurements. Delft, The Netherlands: Delft Hydraulics Laboratory
46. Van Rijn LC (1993) Principles of Sediment Transport in Rivers, Estuaries and Coastal Seas. Aqua Publications, Amsterdam
47. Van Rijn LC (2007) Unified View of Sediment Transport by Currents and Waves. i: Initiation of Motion, Bed Roughness, and Bed-Load Transport. J. Hydraul. Eng. 133 (6), 649–667.
48. Wyss C, Rickenmann D, Fritschi B, Turowski J, Weitbrecht V, Boes R (2016) Measuring bed load transport rates by grain-size fraction using the Swiss Plate Geophone signal at the Erlenbach. J. Hydraul. Eng. 142 (5), 04016003-1-04016003-11.
49. Xia Shen, Ran Li, Huanjie Cai, Jingjie Feng, Hang Wan (2022) Characteristics of secondary flow and separation zone with different junction angle and flow ratio at river confluences, Journal of Hydrology, Volume 614, Part B, 128537, https://doi.org/10.1016/j.jhydrol.2022.128537.
50. Zhang X, Y Ji, Yang Z, Wang Z, Liu N, Jia P (2015) End member inversion of surface sediment grain size in the South Yellow Sea and its implications for dynamic sedimentary environments. Sci. China Earth Sci. 59: 258–267
51. Zhang Z, Lin Y (2021) An experimental study on the infuence of drastically varying discharge ratios on bed topography and fow structure at urban channel confuences. Water 13(9):1147. https://doi.org/10.3390/w13091147

Figures

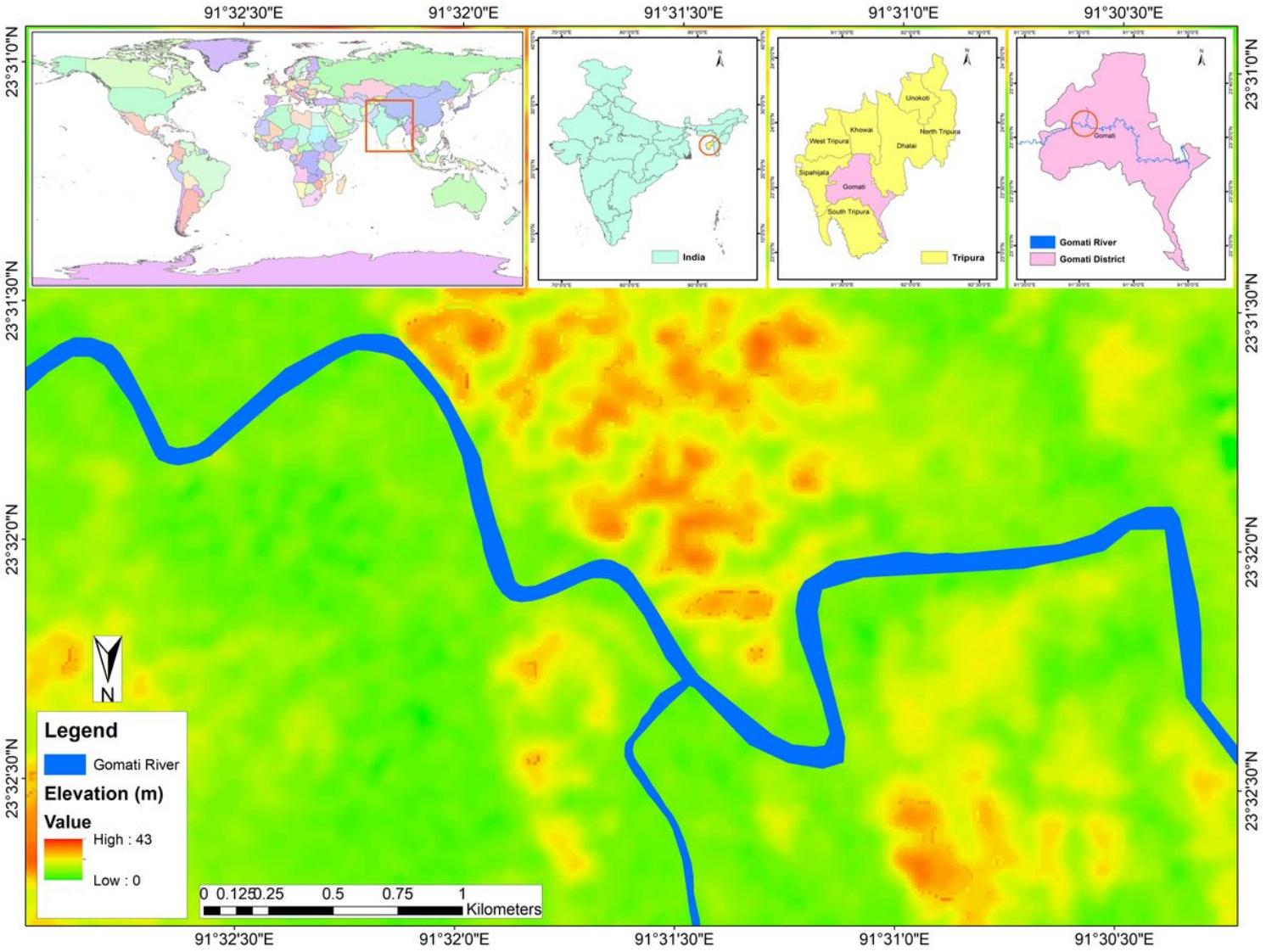

Figure 1

Map of study area (Gumti River Confluence).

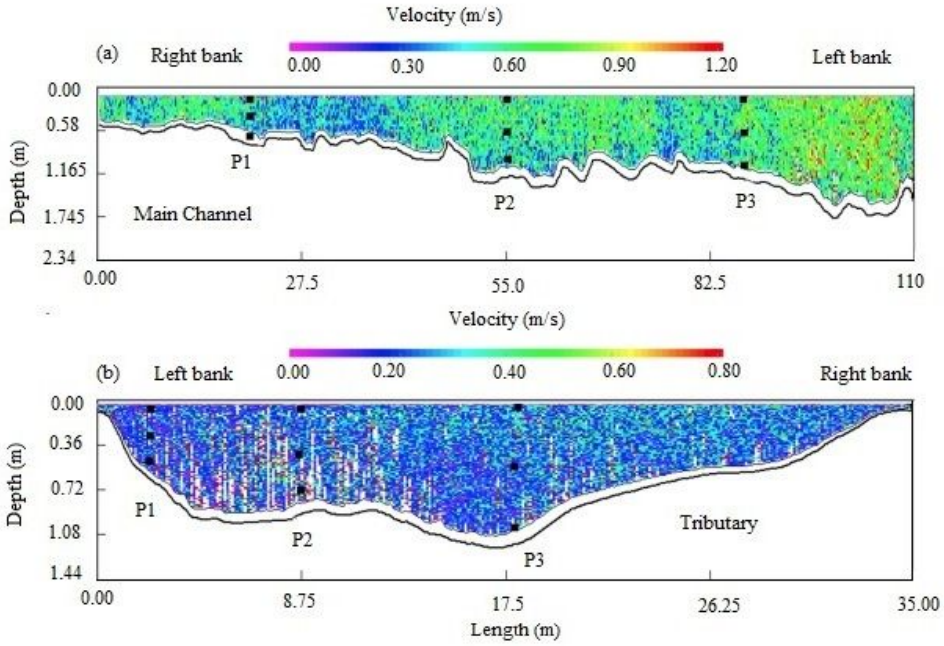

Figure 2

Deep area and shallow area signify the left bank and right banks of both channels (a) main, and (b) tributary, respectively, are conquered during bathymetry survey.

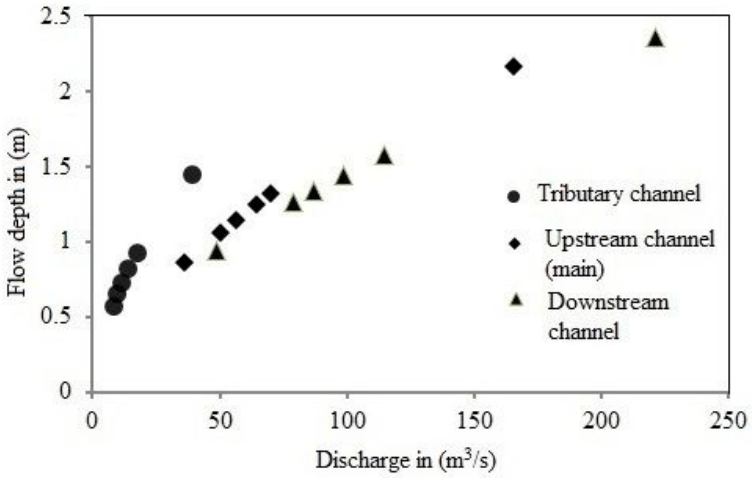

Figure 3

Shows the rating curve relationship between streamflow (discharge) and stage (river water level).

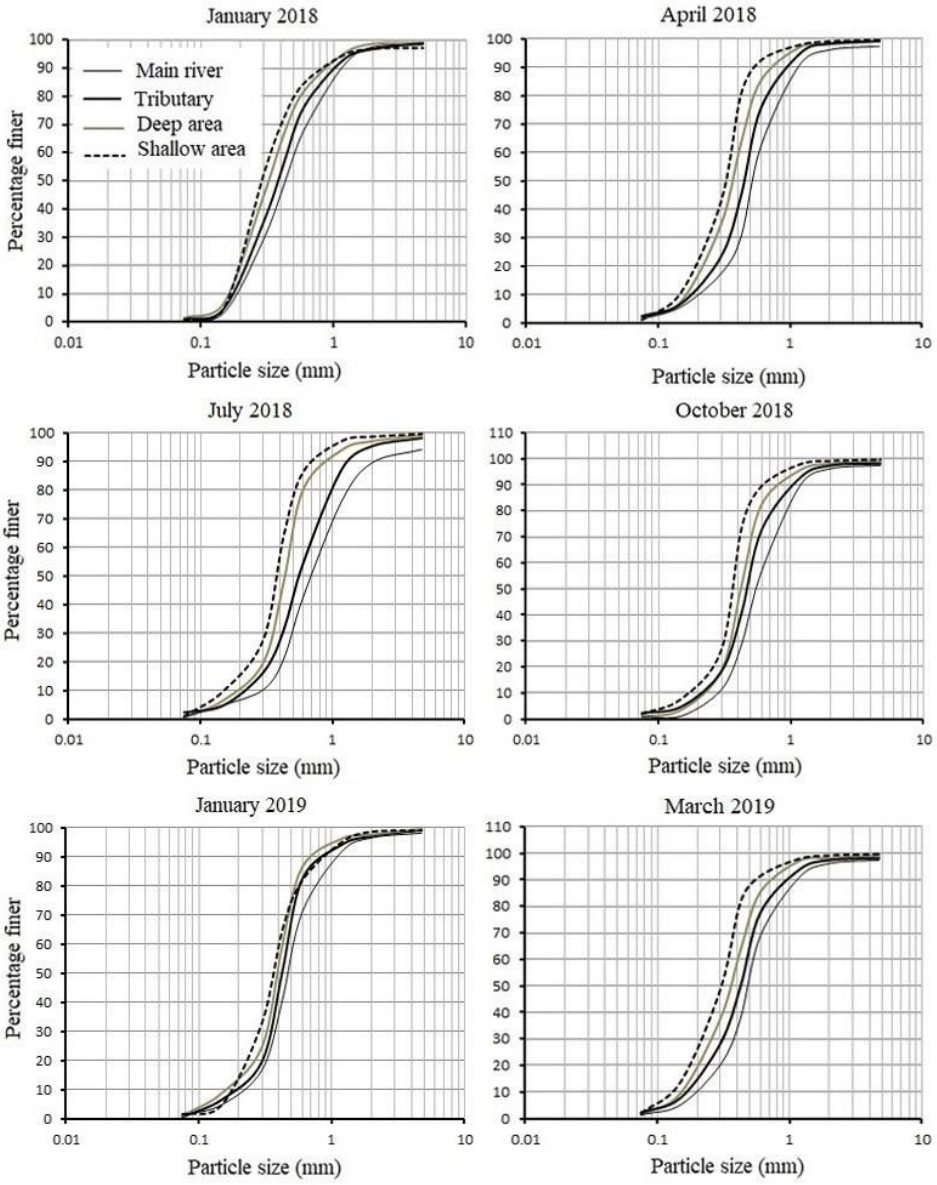

Figure 4

Particle size distribution (PSD) curves of collected samples.

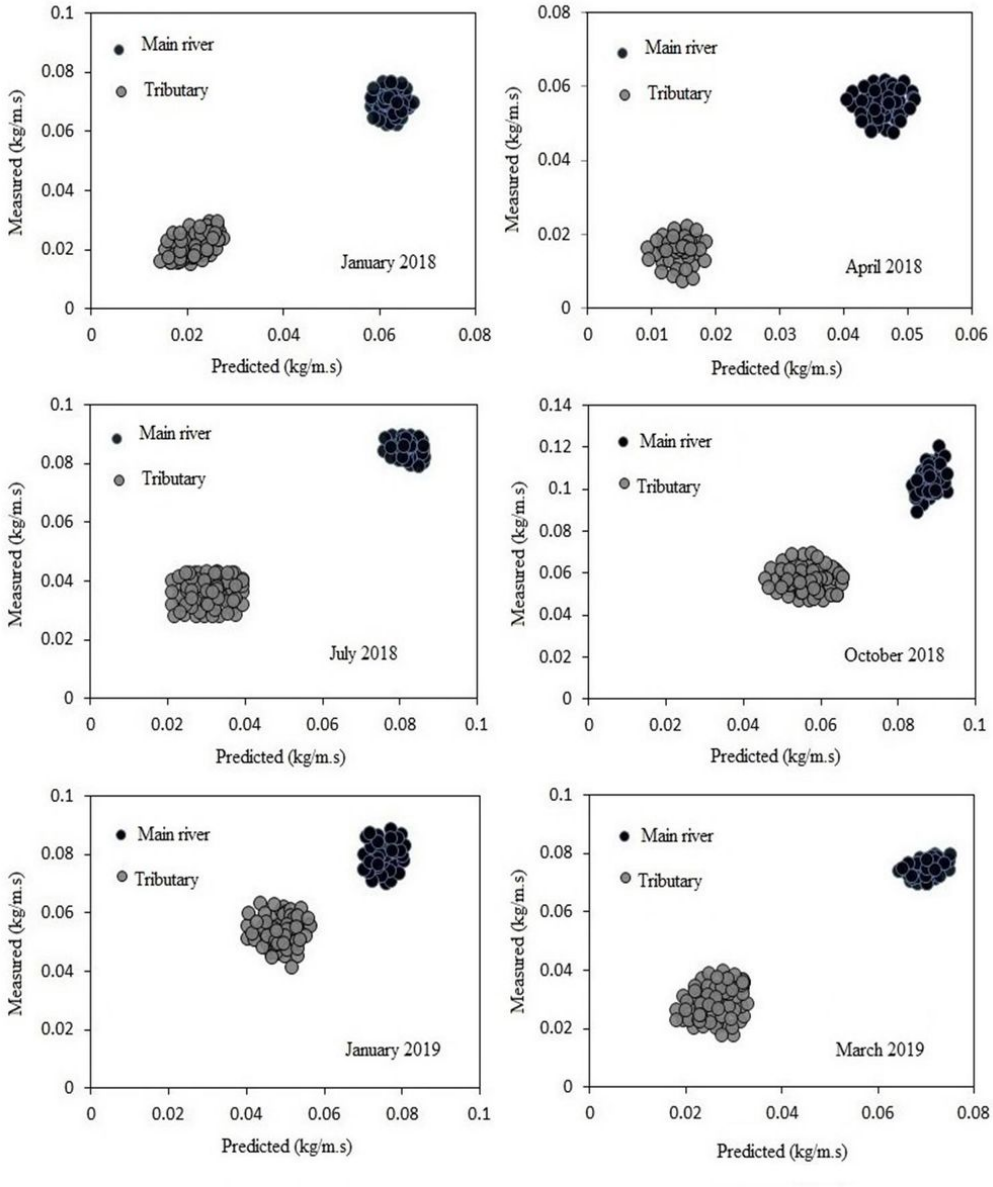

Figure 5

Plot shows the empirical and measured data of unit bedload transport rate for both main channel and tributary.

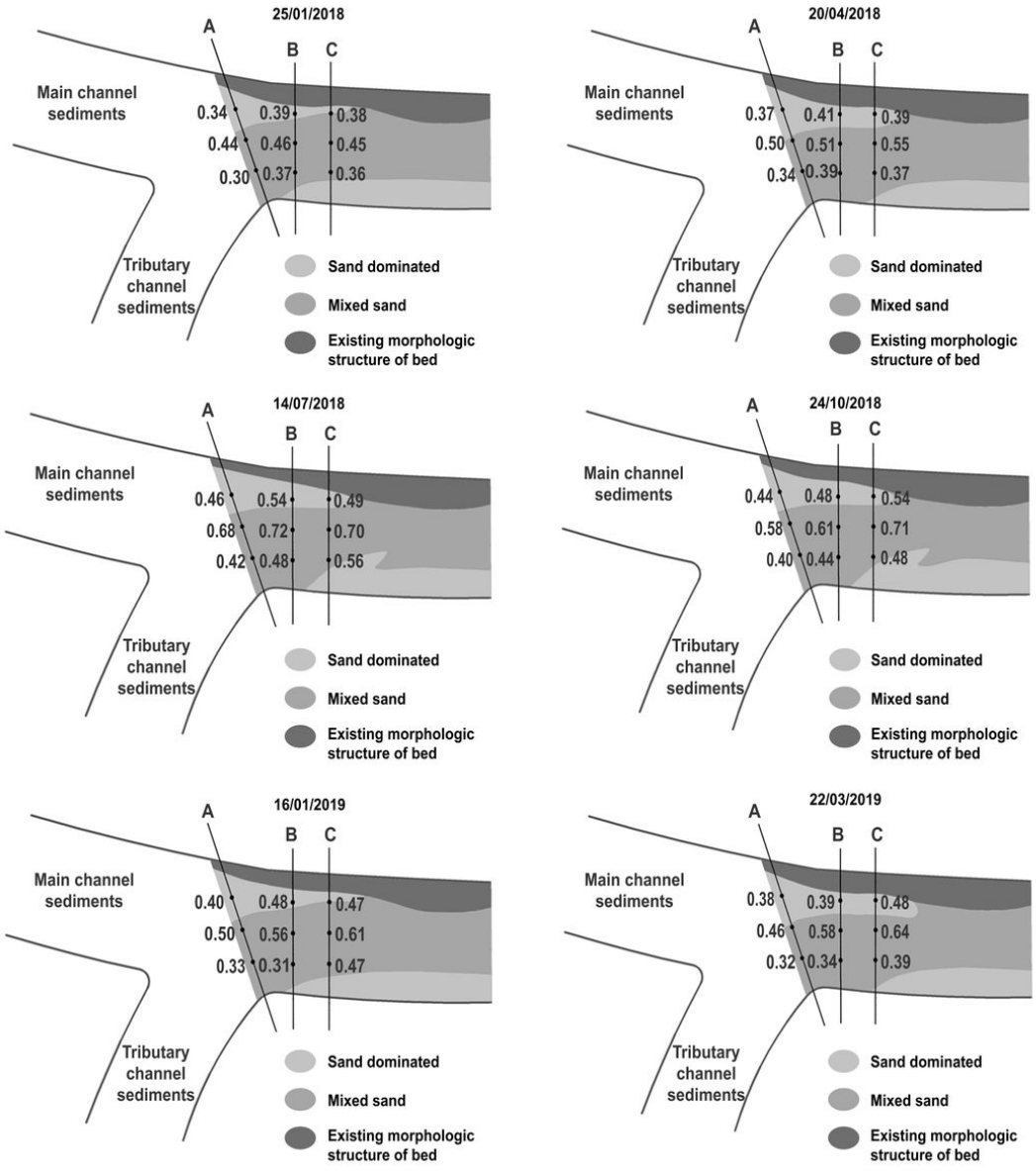

Figure 6

Spatial distribution of bed material on 25 January, 2018; 20 April 2018; 14 July, 2018; 24 October, 2018; 16 January, 2019; 22 March, 2019 (values of median particle size in mm).

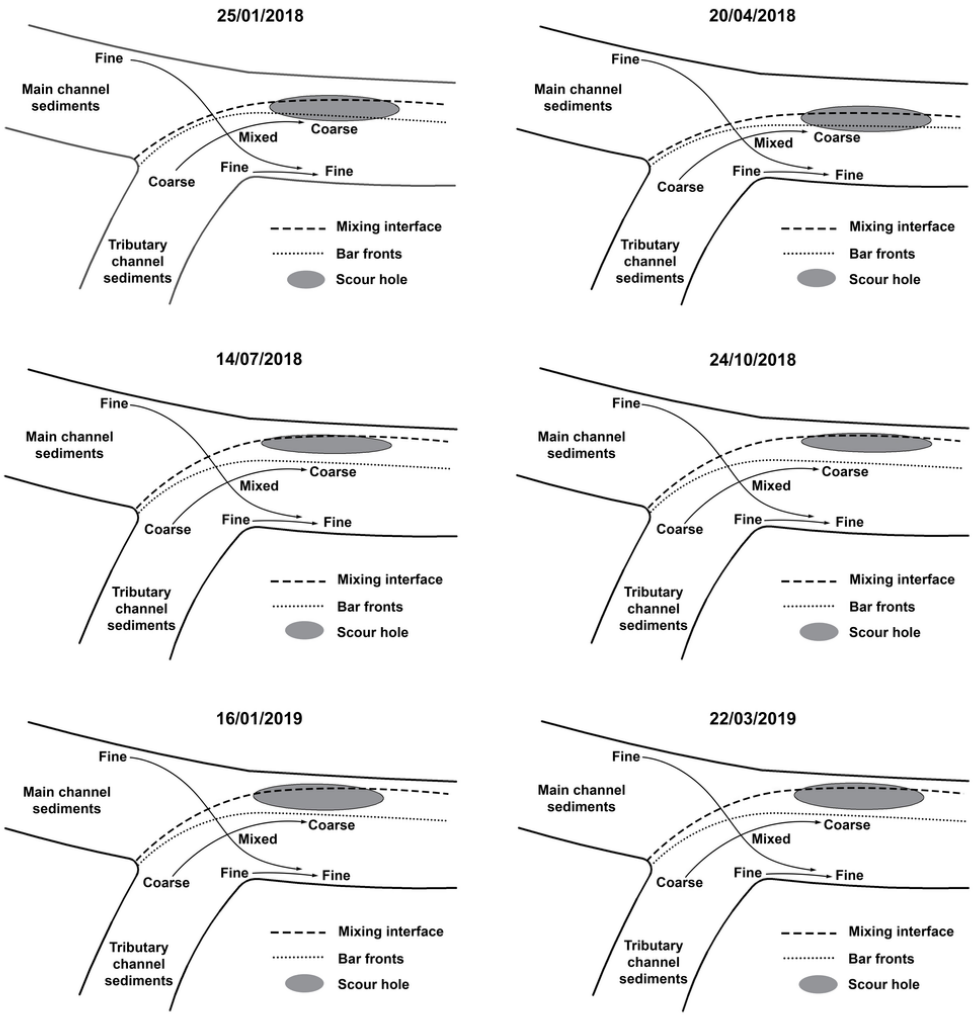

Figure 7

Conceptual model of erosion of surficial material (scour) at an asymmetrical confluence caused by low and high flow situation during (January 2018-March 2019)

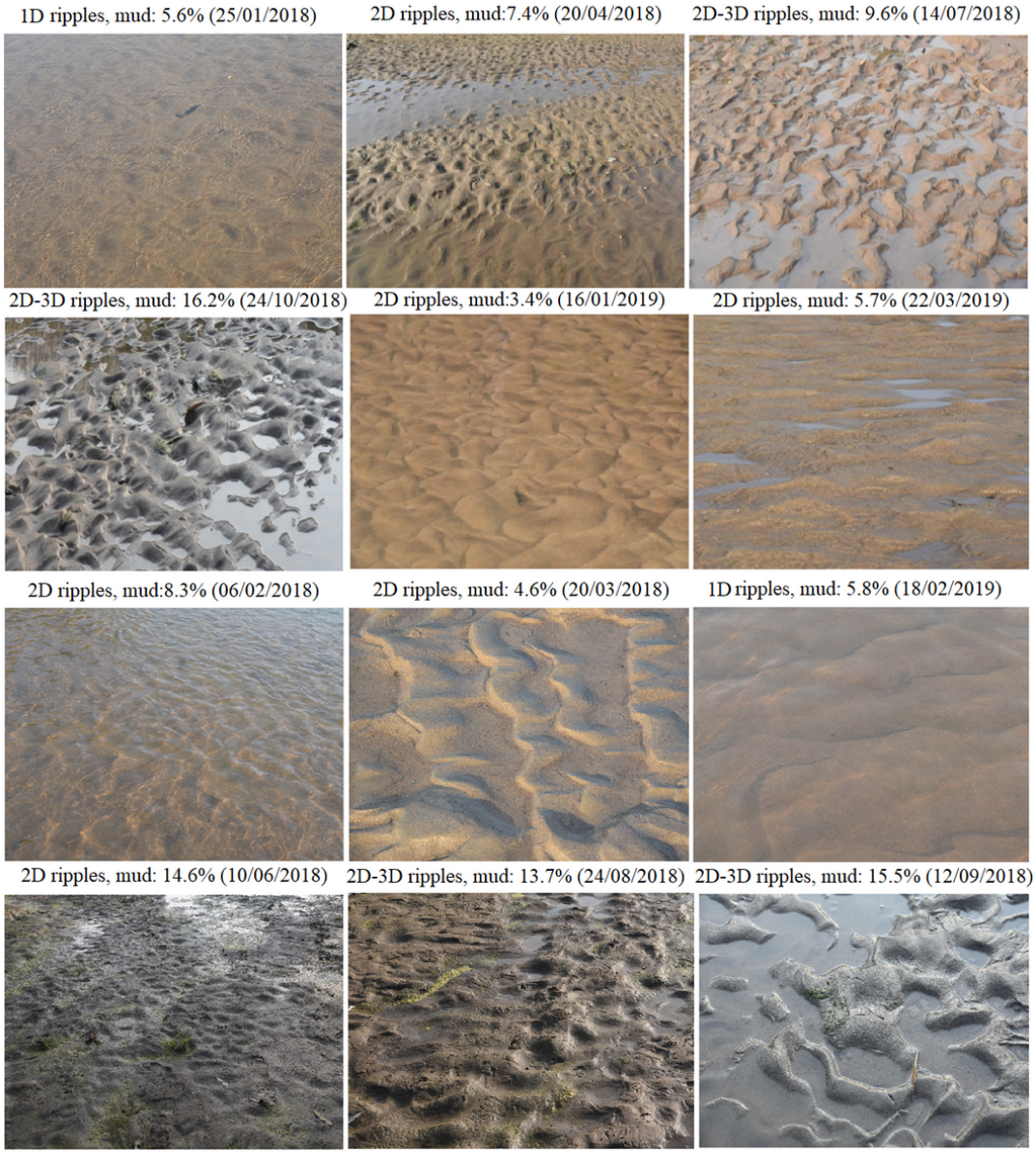

Figure 8

Typical ripple cross-section geometries observed in the field surveys. Ripples were generated under calm and mild wind conditions.

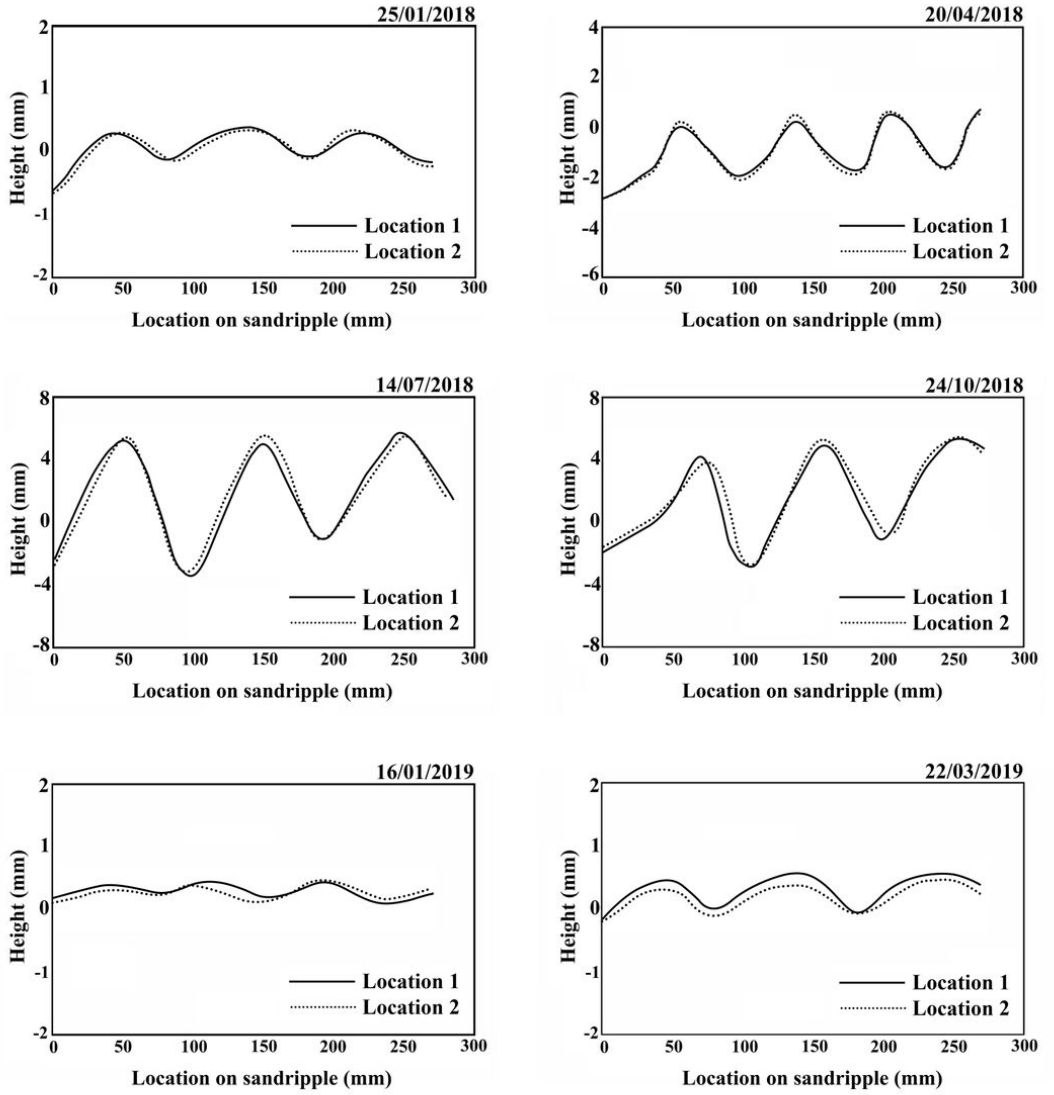

Figure 9

Plan view of ripples acquired at two different locations within the areas have been cropped to ~ $3m^2$ (2 m length × 1.5 m width).

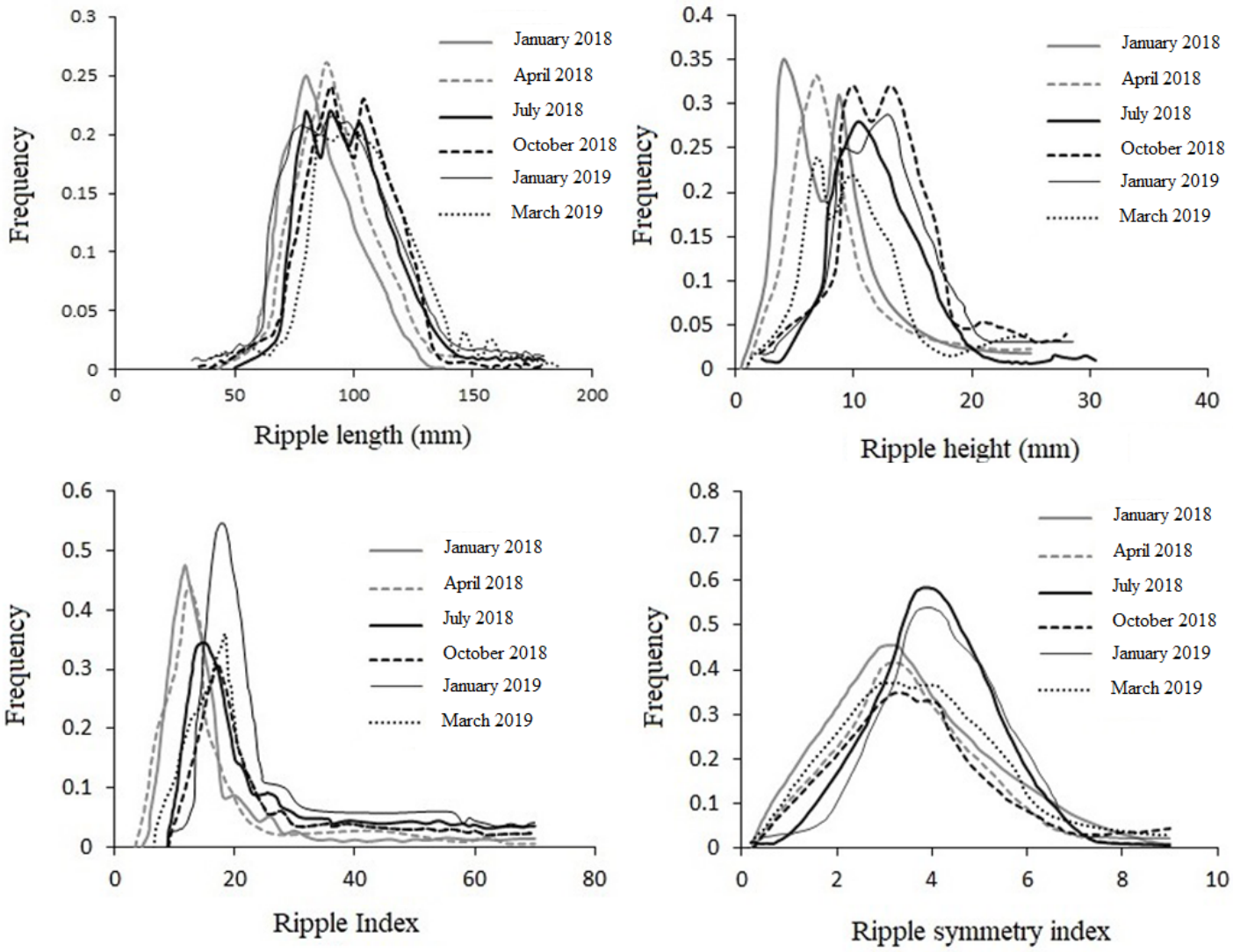

Figure 10

Frequency curves of measured ripple heights; ripple lengths; ripple index; and ripple symmetry index.